Heat recovery with steam compressor: Dynamic model of a superheated steam drying system to evaluate efficient system operation

Michael Poelzl[a], Reinhard Jentsch[a], Johannes Riedl[a], Gregor Schumm[b], Marcel Meinders[c], Felix Hubmann[a], Sabrina Dusek[a]

[a]AIT Austrian Institute of Technology, Giefinggasse 4, 1210 Vienna, Austria
[b]Piller Blowers & Compressors GmbH, Nienhagener Str. 6, 37186 Moringen, Germany
[c]Wageningen University & Research, Droevendaalsesteeg 4, 6708 PB Wageningen, The Netherlands

Abstract

The pulp and paper industry continually seeks innovative technologies to enhance efficiency, reduce energy consumption, and improve product quality. Superheated steam drying (SSD) is a promising alternative to conventional drying methods, offering significant advantages in terms of energy efficiency, environmental sustainability, and product quality. In this contribution, a dynamic model of an SSD system is presented that enables the latent heat recovery at higher temperatures and pressure levels, by using a steam compressor. The steam compressor utilizes the excess steam mass flow from the dryer, upgrading the recirculating superheated steam atmosphere again to target dryer inlet conditions.
However, the integration of SSD technology with existing paper manufacturing processes can be complex and may require substantial modifications to the production line. The innovative nature of SSD necessitates a thorough understanding of its operation to ensure successful implementation.
To address these challenges, a dynamic model simulating the transient behaviour of the paper machine and auxiliary equipment has been developed. This model provides insights into the energy consumption and performance by simulating the interactions between the main process units (dryer, steam compressor) and auxiliary equipment (heat exchanger, electrical heating).
The dynamic model considers the impacts of temperature levels and air in the steam atmosphere. The functionality of the model is shown through selected scenarios and the impact on the efficient operation of the system is analysed.
The dynamic model presented in this study offers a valuable tool for achieving an efficient system design and operating conditions for SSD technology.

Keywords: paper drying; superheated steam drying; steam compressor; dynamic model; process electrification

1. Introduction

The pulp and paper industry is one of the most energy-intensive manufacturing sectors, with the drying section of paper machines accounting for a particularly large share of total thermal energy demand. In 2023, the “paper, pulp and printing” industry accounted for approximately 14.3 % of the EU’s industrial final energy consumption (approximately 1 225 PJ)), being the third biggest final energy consuming industrial sector behind “Chemical and petrochemical” and “Non-metallic minerals” [1]. Within this sector, drying operations typically account for around 60–70% of the total thermal energy consumption [2]. Consequently, improving drying efficiency is essential to meet both economic and environmental targets under the European Green Deal.
Superheated steam drying (SSD) is a promising alternative to conventional air or cylinder drying. Theoretical and experimental studies have shown that SSD offers several advantages, including higher heat-transfer coefficients, improved drying rates, elimination of exhaust air, and the potential for closed-loop operation that allows effective heat recovery [3,4]. In an industrial context, the integration of SSD with latent heat recovery - such as through the use of a steam compressor - can enable substantial reductions in primary energy use and carbon emissions [2].

15th IEA Heat Pump Conference 2026 - AIP2.4 - https://doi.org/10.23697/tvgs-ak27

Nevertheless, despite these potential benefits, large-scale implementation of SSD remains limited due to several operational and integration challenges. In their experimental work, Kiiskinen and Edelmann [5] demonstrated that SSD of paper webs can achieve high drying rates and effective energy recovery, but they also identified practical constraints including maintaining airtightness, ensuring high steam purity, and managing condensation and two-phase flow behaviour. They further emphasised that transient effects - such as temperature and pressure fluctuations during start-up and disturbances - must be better understood to ensure stable operation and product quality. Similar challenges have been discussed by Mujumdar [3] who pointed out that non-condensable gases, fouling, and dynamic instability remain key barriers to industrial deployment.

These findings indicate that the successful industrial adoption of SSD requires a deeper understanding of its dynamic behaviour. Unlike steady-state process models, a dynamic approach allows the temporal evolution of temperature and mass flow within the closed-loop system to be analysed. This is particularly relevant when considering auxiliary systems such as steam compressors and heat exchangers, where transient effects influence the overall energy efficiency. A dynamic model enables an analysis of different operational scenarios, thereby providing a quantitative basis for assessing whether the achievable energy savings and drying performance are competitive with conventional drying technologies.

Therefore, a dynamic model of an SSD drying system with an integrated steam compressor for heat recovery has been developed in Modelica/Dymola [6]. The model captures the coupled thermal and mass-flow behaviour of the main process components and incorporates practical phenomena such as air ingress and variable drying temperatures.

By simulating time-dependent operating conditions, the model serves as a quantitative tool for evaluating system performance, energy efficiency and recovery potential. This approach provides both a methodological advancement and a practical basis for insights into the SSD technology in the paper industry, thereby supporting the transition from laboratory-scale demonstrations to full-scale industrial implementation.

2. Methods

2.1. System layout

The investigated system consists of a closed-loop superheated steam drying configuration equipped with a steam compressor and heat exchanger for heat recovery and is depicted in Fig. 1. Wet paper and superheated steam enter the dryer, allowing water from the paper to evaporate into the surrounding steam atmosphere. A part of the resulting steam is directed to a steam compressor (mechanical vapour recompression) unit, where it is compressed to a higher pressure and temperature. This upgraded steam then passes through a heat exchanger, reheating the circulating steam atmosphere before re-entering the dryer. An electric heater is included downstream of the heat exchanger to control the temperature to the target drying temperature, ensuring stable operation under varying load conditions.

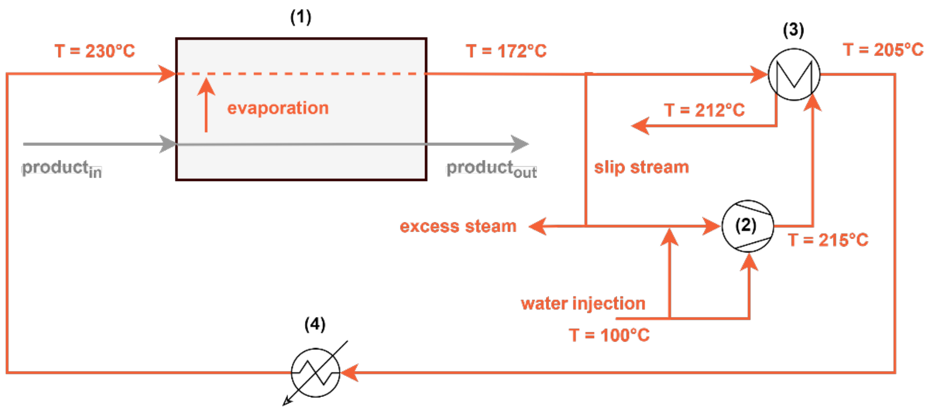

Figure 1. System layout of a closed loop superheated steam dryer, with drying section (1), mechanical vapour recompression (2), heat exchanger (3) and electrical heater (4). (The temperature levels are shown for the reference case, described in section 2.3.1.)

2.2. Dynamic model

The system described in Section 2.1 is modelled in Modelica/Dymola [6] using and expanding on the TIL library [7]. The superheated steam atmosphere was modelled as a gas mixture of steam and dry air to be able to consider a certain amount of air in the steam flow that can occur, for example, due to leakages.

Moreover, the media flow was expanded to include particles. This particle loading can be used to model fouling in heat exchangers or for investigating the influence of cleaning units.

As already mentioned in Section 2.1, the excess steam produced during drying is fed into a steam compressor. Before it enters the steam compressor, water at 100°C is injected to ensure saturation at the steam compressor inlet. Furthermore, it was assumed that, depending on operating conditions, the heat recovery system (steam compressor and heat exchanger) may not be able to provide the necessary dryer inlet temperature. Therefore, an electric heating element is included in the model. This element is modelled as a heat source, with the power requirement calculated at an assumed efficiency of 0.99.

The three main components of the dynamic model - dryer, steam compressor and heat exchanger - are explained in more detail in the following subsections.

2.2.1. Dryer

The dryer model makes full use of the object-oriented component-based capabilities of the Modelica modelling language. The dryer has inlet and outlet connections for gas and solid flows. Inside, the gas and solid are modelled in two distinct phases with interaction transport terms between them, depicting drying rate, fouling rate and heat flow rate. The relevant properties are modelled in differential balances according to Equation (1)-(4) with additional equations constraining the overall mass balances for solids, Equation (5), and for gas, Equation (6). The balanced properties are

- For energy balances: Specific enthalpy for gas $h_g = f(x_{w,g}, T_g)$ and solid $h_s = f(x_{w,s}, T_s)$
- For component balances: Gas composition mass fractions $x_{w,g}$, water loading on dry solid $x_{w,s}$ and solid loading on gas x_s;
- The transfer rates are: $\dot{Q}$ the heat transfer rate, F the fouling rate and J the drying rate accordingly.

$$\frac{d(h_g \cdot m_g)}{dt} = \dot{m}_{g,in} \cdot h_{g,in} - \dot{m}_{g,out} \cdot h_{g,out} - \dot{Q} + J \cdot h_w \tag{1}$$

$$\frac{d(h_s \cdot m_s)}{dt} = \dot{m}_{s,in} \cdot h_{s,in} - \dot{m}_{s,out} \cdot h_{s,out} + \dot{Q} - J \cdot h_w \tag{2}$$

$$\frac{d(x_{w,g} \cdot m_g)}{dt} = \dot{m}_{g,in} \cdot x_{w,g,in} - \dot{m}_{g,out} \cdot x_{w,g,out} + J \tag{3}$$

$$\frac{d(x_{w,s} \cdot m_s)}{dt} = \dot{m}_{s,in} \cdot x_{w,s,in} - \dot{m}_{s,out} \cdot x_{w,s,out} - J \tag{4}$$

$$\dot{m}_{s,dry,in} - \dot{m}_{s,dry,out} - F = 0 \tag{5}$$

$$\dot{m}_{g,in} - \dot{m}_{g,out} - J = \frac{\partial \rho_g}{\partial t} \cdot V_g \tag{6}$$

Further $m_{g|s}$ is the respective gas or solid mass, $\dot{m}_{g|s}$ the inlet and outlet flows, h_w the specific enthalpy of water, ρ_g the gas density, V_g the gas volume. As the solid and gas is modelled as two component phases – water and solid or water and air – Equations (1)-(6) provide a closed system for all components.

The calculation of the transport rates J and $\dot{Q}$ between the paper and the gas is considered using a driving force approach for heat and mass transport, using Equation (7) and Equation (8) respectively.

$$\dot{Q} = \alpha A \cdot (T_g - T_s) \tag{7}$$

$$J = \beta A \cdot \left(\rho_{w,s} \cdot \phi(x_{w,s}, T_s) - \rho_{w,g}\right) \tag{8}$$

Here, A is the surface area between the gas and the paper, α is the convective heat transfer coefficient, and β is the mass transfer coefficient. The terms T_g and T_s denote the gas and solid paper temperatures, while $\rho_{w,g}$ and $\rho_{w,s}$ correspond to the partial densities of water in the gas phase and at the paper surface, respectively. $\phi(x_{w,s}, T_s)$ is a correction for the water sorption in the paper in accordance with [8].

To determine the heat and mass transfer coefficients, a Nusselt and Sherwood number correlations for round nozzle jet impingement, as recommended by the VDI Heat Atlas [9], are applied.

2.2.2. Steam compressor

The steam compressor model development is based on manufacturer's simulation data of various steam compressor systems designed for pure saturated steam with a suction pressure of 1.05 bar_a, and a steam outlet pressure of 20 bar_a. All simulated steam compressor systems consist of multiple radial turbo compressors in series. The manufacturer's simulation data was condensed into characteristic polynomials depending on steam compressor speed for pressure increase, temperature increase, specific shaft power and water injection mass flow and were later normalized by the maximum mass flow of different compressor system designs (15, 25 and 40 tons/h). Furthermore, machine learning approaches - mainly nonlinear data preprocessing and elastic-net regularisation for regression training as proposed by [10] were used to fit the data generated by these characteristic polynomials to the target values speed and energy consumption with inlet mass flow and pressure lift as input variables. These two functions were implemented in the steam compressor model. The water injection mass flow is controlled so that a superheating of 2.5 K occurs at the steam compressor outlet based on thermo-physical calculations.

To consider the influence of the air content in the steam mass flow, a correction equation for shaft power was created as a function of the air content based on provided manufacturer data and included in the model. In general, the energy requirement of the steam compressor decreases as the proportion of air in the steam mass flow increases. The maximum allowed air content of the suction steam in the model is 12%, as the real steam compressor system behaves fundamentally differently compared to the abstracted data-driven dynamic model with higher air contents in the steam flow. For this contribution an electrical motor efficiency of 0.92 is assumed for the compressor.

2.2.3. Heat exchanger

As shown in Fig. 1 a heat exchanger is included in the system. In the heat exchanger steam condenses on one side (hot side) and superheated steam is heated on the other (cold side). A fin and tube heat exchanger type was selected for this application. Therefore, the heat exchanger model available in the TIL library was used and further developed. This model includes the geometry and mass of the component (e.g. heat capacity of wall and fins can be considered). Discretisation in finite volumes accounts for spatial effects, e.g. the change of moisture contents and therefore thermal properties due to condensation. No pressure losses were considered for the investigations presented in this paper, and different correlations provided and referenced in the TIL library were used in the model to calculate the heat transfer coefficients. On the tube side for the gaseous single phase (steam cooling) the correlation proposed by Gnielinski, Dittus and Boelter [11] was chosen and for condensation the correlation proposed by Shah [12] was chosen. Those are then weighed proportional to the amount of gaseous single phase in each cell (see Equation (9)). The fraction q as described in Equation (10) is used as drop-in replacement for the steam quality number – that defines the two-phase region – in the TIL library default implementation. On the fin-side the correlation by Haaf [13] was used to calculate the heat transfer coefficient.

$$\alpha_{Tube} = w(q) \cdot \alpha_{GDB} + (1 - w(q)) \cdot \alpha_{Shah} \tag{9}$$

$$q = \frac{x_{w,g}}{x_{w,g,in}} \tag{10}$$

2.3. Scenarios

To assess the influence of operating parameters and disturbances, two simulation scenarios are defined. Each case covers a specific effect - temperature variation and air leakage - enabling an evaluation of their impact on energy efficiency, heat transfer, and system behaviour compared to the reference operation.

2.3.1. Reference Case

In the assumed reference case, the drying process operates under fully convective conditions, where the circulated superheated steam is blown through an array of nozzles to dry the moving paper web. For the steam compressor an upper pressure limit of 20 bar_a was assumed. Not the entire slip stream is used for heat recovery: Instead, the heat recovery for this case was specifically designed such that the fraction of the slip stream directed through the compressor and the geometry of the heat exchanger ensure that 90% of the mass flow condenses within the heat exchanger, while the circulating atmosphere reaches a temperature of 205 °C at the heat exchanger outlet.. Relevant information to the reference case can be found in Table 1.

Table 1: Reference case

	Value	Unit
Drying Temperature	230	°C
Circulating Steam Mass Flow	178	kg/s
Paper Inlet Temperature	35	°C
Solid Paper Mass Flow	10	kg/s
Paper Inlet Dry Content	50	%
Evaporated Water Mass Flow (Drying Capacity)	8.91	kg/s
Mass Flow To Steam Compressor	4.45	kg/s
Pressure Steam compressor Outlet	20	bar_a
Power Consumption Steam compressor	4 604	kW
Total Power Consumption	13 824	kW

2.3.2. Scenario 1: Change of Drying Temperature

In the first scenario (see Fig. 2), the drying temperature is lowered to 210°C. This leads to an expected drop in evaporated mass flow. Therefore, the circulating volume flow entering the dryer must be ramped up – leading to higher mass and heat transfer – to again ensure similar evaporation rates. Just as in the reference case, the mass flow over the steam compressor is adjusted for a 12 K pinch over the heat exchanger, while the heat exchanger geometry stays the same.

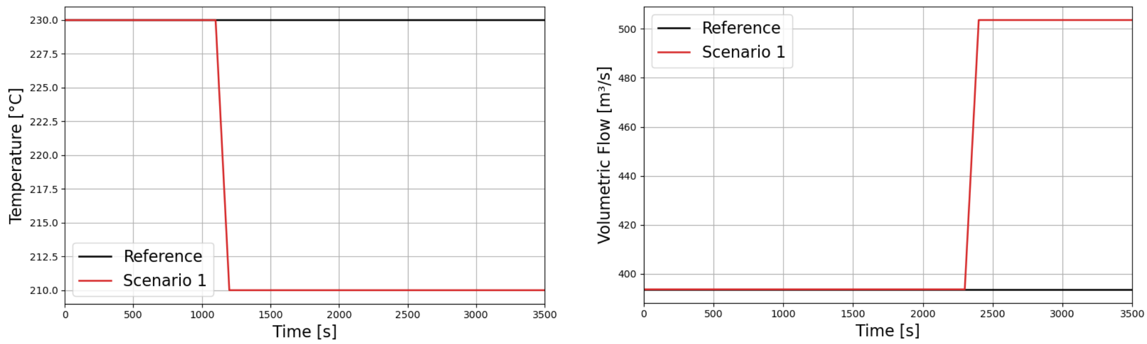

(a) (b)

Figure 2. Inputs Scenario 1: (a) Drying Temperature and (b) Circulating volume flow over time.

2.3.3. Scenario 2: Air Leakage

In the second scenario, the effect of air infiltration into the dryer is investigated. The introduction of air alters the composition of the gas phase, which is expected to impact drying rates, steam compressor operation, and heat transfer performance within the heat exchanger.

To analyse these effects, a leakage rate of 1 kg/s of air entering the dryer is simulated. This leads to an air content of about 10% in the circulating drying atmosphere. Two different inlet air temperatures are considered to separate the influence of temperature from that of gas composition: one scenario assumes air at 230 °C, while the other represents ambient (hall) air at 25 °C. For comparability, the mass flow over the steam compressor stays the same as in the reference case with heat exchanger geometry also remaining the same. Additionally, the circulating volume flow is modified to achieve the same final moisture content of the paper as in the reference case.

3. Results

3.1. Scenario 1: Change of Drying Temperature

In Scenario 1, the drying temperature is reduced at t=1100 s from 230°C to 210°C, as shown in the temperature input profile in Fig. 2 (a). This change is implemented to analyse its impact on the drying process and energy consumption of the system.

Fig. 3 shows that the reduction in drying temperature leads to a drop in the mass flow of evaporated water, decreasing from 8.91 kg/s, after a transient period, to the new steady state of around 7.27 kg/s after the temperature change. This decline reflects the reduced thermal energy available for evaporation, directly impacting the drying process. However, the mass flow of evaporated water recovers when the volumetric flow rate increases at t=2300 s.

The power consumption of the steam compressor and the total power demand of the system in Fig. 3 are affected by the temperature change. The total power consumption, which includes both the steam compressor and electrical heater, decreases during the lower temperature phase. However, when the volumetric flow rate increases at 2300 seconds, both the steam compressor and total power consumption rise again, reflecting the higher workload required to maintain the drying process under the new conditions.

The results demonstrate that reducing the drying temperature leads to a temporary decline in drying performance, as evidenced by the decreased mass flow of evaporated water and lower power consumption. The subsequent increase in volumetric flow rate compensates for this effect, resulting in a surge in power demand. This scenario underscores the sensitivity of the drying process to temperature variations and highlights the importance of optimizing both temperature and flow rate to achieve energy-efficient operation.

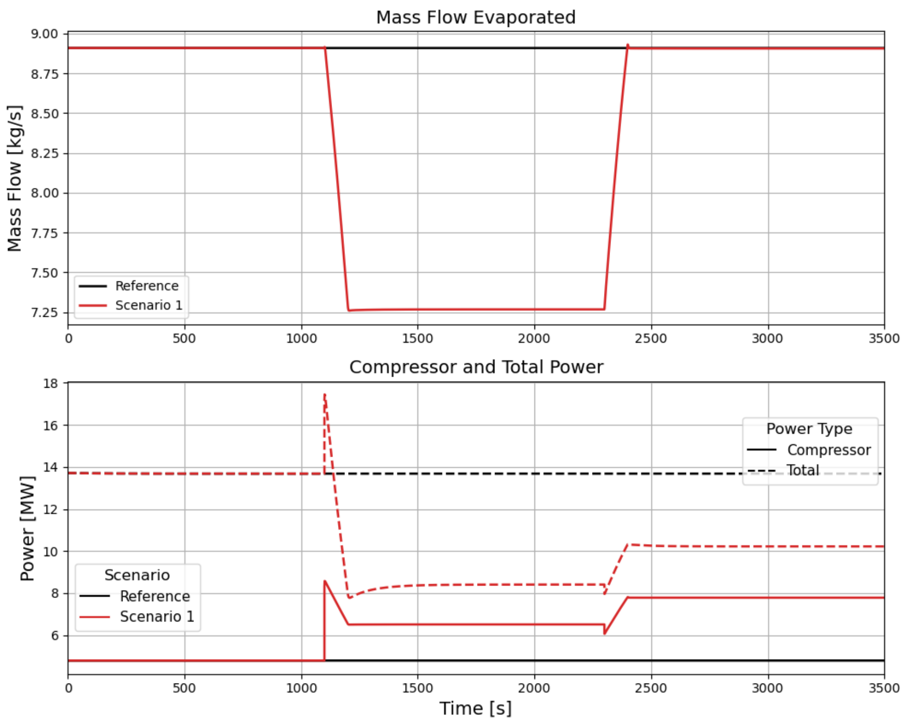

Figure 3. Results Scenario 1: Evaporated Mass Flow (above) and power consumption of steam compressor as well as steam compressor and electric heater combined (below).

The findings are summarised in Fig. 4. The power consumption of steam compressor and electrical heater are taken from steady-state periods, resulting in three distinct periods to be compared: the reference, period 1 (t = 1500 - 2300s) with lowered drying temperature, and period 2 (t=2700-3500 s) with lowered drying temperature and increased volume flow.

In the reference period, the electrical heater accounts for 65.0% of the total power needed. It's obvious that in this drying temperature range the system is relying to a big extent on the electrical heater to maintain the drying temperature since the selected steam compressor for this system is not able to provide the desired temperature level.

For period 1, the total power consumption decreases to 61.4% of the reference. This reduction in total power consumption reflects the lower thermal energy requirement due to the decreased drying temperature. The main contributor here is the steam compressor, operating at a favourable temperature level. Since the outlet temperature of the dryer is lower under reduced drying temperature conditions, a higher mass flow through the compressor – 6.05 kg/s instead of 4.45 kg/s - is required to maintain the target temperature of 205 °C at the heat exchanger outlet. Consequently, the share of steam compressor energy consumption increases.

In period 2, the total power consumption rises to 74.7% of the reference. Both, steam compressor and electrical heater show increased power demand compared to period 1, attributed to the increased volume flows both have to handle.

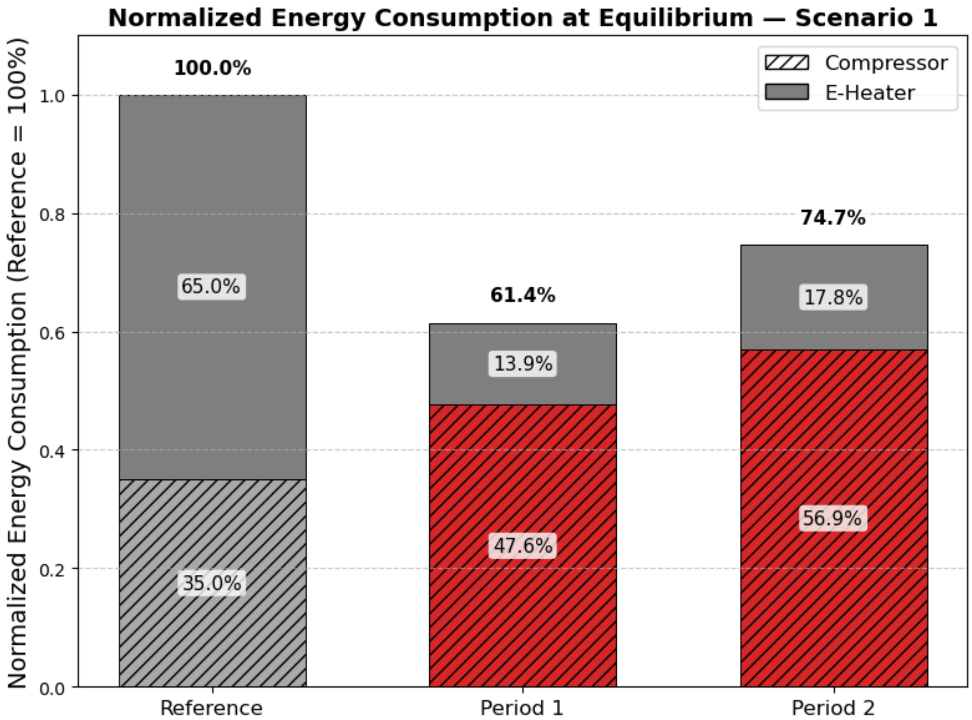

Figure 4. Normalized power of steam compressor and electric heater for period 1 (lowered drying temperature) and period 2 (lowered drying temperature, higher volume flow) in Scenario 1.

3.2. Scenario 2: Air Leakage

Fig. 5 and Fig. 6 illustrate the transient response of the heat pump dryer system for three configurations: the reference case without leakage, a leakage of cold ambient air, and a leakage of hot air at steam temperature.

In the upper part of Fig. 5, the mass flow of evaporated water increases following the introduction of air leakage. To achieve the same final moisture content of the paper as in the reference case, the circulating volume flow was adapted. This leads to a lowered evaporated mass flow before the introduction of air into the dryer.

The lower part of Fig. 5 makes it evident that the introduction of colder air results in a lower dryer outlet temperature.

The power traces in Fig. 6 reveal that the steam compressor power decreases for the same mass flow to the compressor as in the reference case in both leakage scenarios while the overall power consumption of the system increases.

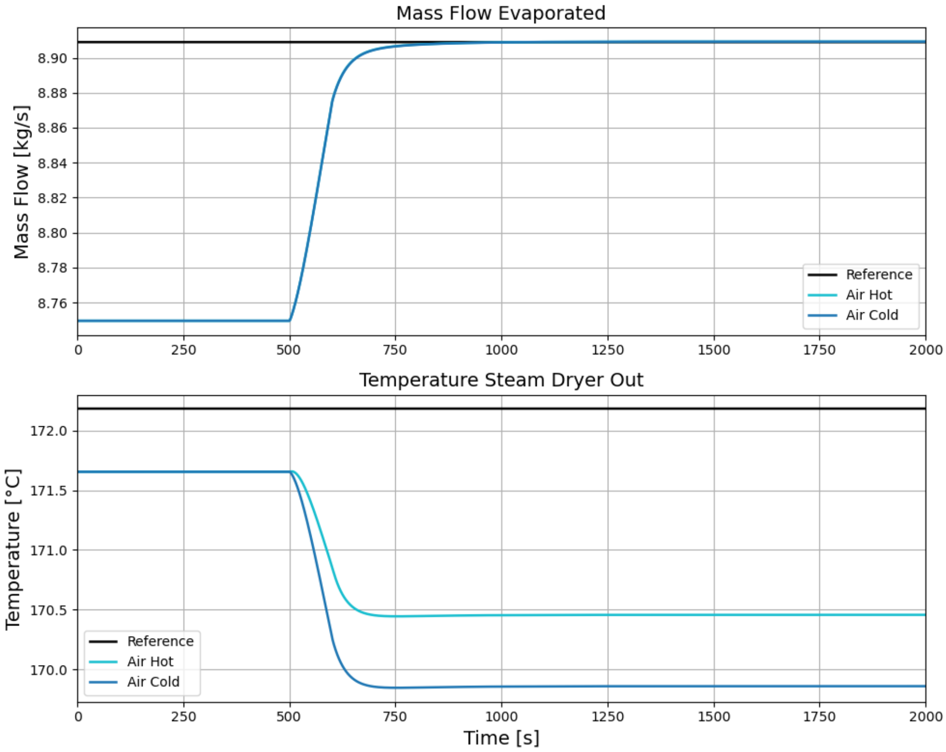

Figure 5. Results Scenario 2: Evaporated Mass Flow (above) and Temperature of steam at dryer outlet (below).

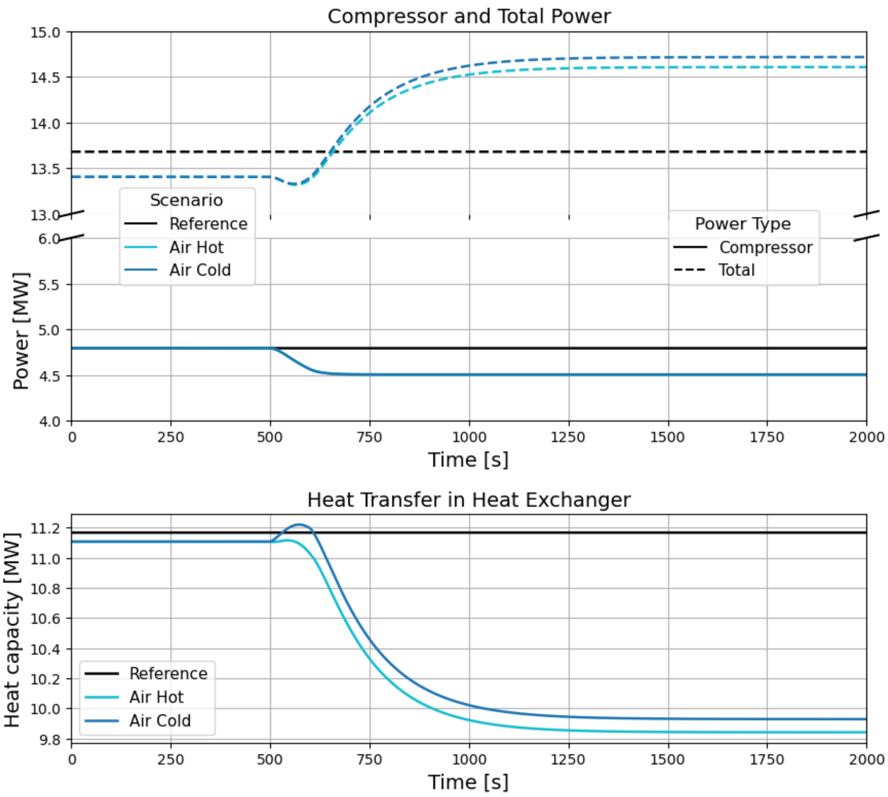

Figure 6. Results Scenario 2: Power consumption of steam compressor as well as steam compressor and electric heater combined (above) and Heat transfer in heat exchanger (below).

This compensating effect is evident in the lower diagram of Fig. 6, which depicts the heat capacity of the heat exchanger. The introduction of non-condensable air leads to a pronounced decrease in recovered heat. As a result, the heat exchanger transfers less energy from the compressed side to the circulating flow, reducing its overall heat capacity. The reduction is more substantial for the hot-air leakage case, as the incoming air lifts the inlet temperature to the heat exchanger, diminishing the available temperature gradient and thus the heat transfer efficiency. Consequently, a larger fraction of the heat demand must be supplied by the electrical heater, increasing its power contribution in this case. Another approach would be to increase the heat exchanger surface area which remains untouched throughout the scenario though.

Fig. 7 summarizes – like in Scenario 1 - the power consumption at equilibrium of the steam compressor and electric heater for three cases: the reference operation without air leakage, leakage of cold ambient air, and leakage of hot air at steam temperature. The values are again normalized with respect to the reference case to enable a relative comparison.

Introducing air leakage into the dryer alters the thermodynamic balance of the system. The presence of air in the steam reduces the heat transfer performance of the existing heat exchanger by lowering the effective steam partial pressure and hindering condensation. As a result, the achievable heat duty decreases (see Fig. 6). Due to this reduced thermal load, the steam compressor handles a lower effective steam mass flow, which leads to a reduction in total compressor power consumption.

However, the increased air fraction also limits the overall heat transfer capacity of the heat exchanger. As a result, a larger portion of the total heat demand must be supplied by the electrical heater. This is reflected in the higher electrical heating power observed for both air leakage scenarios.

Overall, the total power consumption (steam compressor and electrical heater) is higher for the leakage cases than for the reference case. This finding highlights the sensitivity of the system's energy performance to air infiltration and underlines the importance to take these effects into account when designing the system. Validation of the dryer model is planned, as are further investigations into the optimal system design for the air content occurring in a real process.

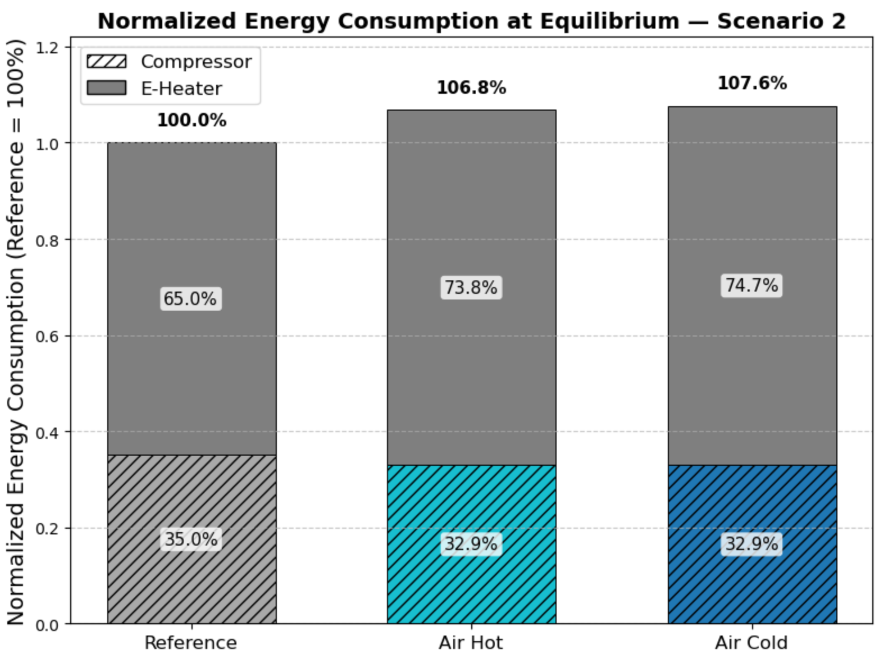

Figure 7. Normalized power of steam compressor and electric heater for different air leakages in Scenario 2.

4. Conclusion and outlook

The investigation of the drying temperature, volume flow, and air leakage scenarios reveals the strong interdependence between process parameters, thermodynamic behaviour, and overall energy efficiency in steam drying systems.

In Scenario 1, a reduction in drying temperature temporarily decreases the evaporation rate and the overall power demand of the system. A subsequent increase in volumetric flow rate compensates for this deficit, resulting in a short-term recovery of drying performance. However, an increased gas flow rate entails higher system requirements - including larger dryer dimensions, additional nozzle capacity, and greater pressure losses within the circulation loop.

The results in Scenario 2 confirm that air leakage disturbs the thermal balance within the system. The reduced heat recovery in the heat exchanger necessitates greater electrical heating, leading to a net increase in total energy demand for the chosen system design. This finding shows the viability of system's energy performance is relying on effective design tailored to real operating conditions. The interplay between the steam compressor and the selection of a suitable heat exchanger including its sizing presents further potential for optimization to enhance energy efficiency.

From a design and operational perspective, the results underscore the importance of holistic modelling in the energetic optimization of steam drying processes. While steady-state efficiency is a viable approach, this study demonstrates that transient processes—such as temperature adjustments, load ramping operational transitions - significantly influence system stability, heat losses, heat recovery and energy efficiency. To accurately predict performance and guide efficient operation, future modelling efforts should prioritize the inclusion of more dynamic scenarios like start-up and shutdown, ensuring that transient behaviour is faithfully represented. Ultimately, such advancements will contribute to the development of energy-efficient and robust drying systems tailored to real-world operational variability.

In a next step, the validity of the drying model will subsequently be examined and validated through experimental trials conducted on a test rig.

5. Nomenclature

Roman symbols

A	surface area between the gas and the paper, m²
f	function
F	fouling rate, kgs^{-1}
h	specific enthalpy
J	drying rate, kgs^{-1}
m	mass, kg
$\dot{m}$	mass flow, kgs^{-1}
q	steam quality, -
$\dot{Q}$	heat transfer rate, W
$\dot{R}_\varepsilon$	drying rate, kgs^{-1}; heat transfer rate, W; fouling rate, kgs^{-1}
T	temperature, K
t	time, s
V	volume, m³
w	weighting factor, -
x	mass fraction, -

Greek symbols

α	heat transfer coefficient, $Wm^{-2}K^{-1}$
β	mass transfer coefficient, m^2s^{-1}
ρ	density, kgm^{-3}

Subscripts

dry	dry

g	gas
GDB	Gnielinski, Dittus and Boelter
in	incoming
out	outgoing
s	solid
Shah	Shah
tube	tube side
w	water

Acknowledgements

This contribution is part of the SteamDry Project. This project has received funding from the European Union's Horizon Europe research and innovation programme under grant agreement No GA 101137906. Views and opinions expressed are however those of the author(s) only and do not necessarily reflect those of the European Union. Neither the European Union nor the grating authority can be held responsible for them.

References

[1] Eurostat. Disaggregated final energy consumption in industry by NACE Rev. 2 activity – quantities. [Online]. Available: https://ec.europa.eu/eurostat/web/energy/database. [Accessed 08 10 2025].
[2] EHPA&Cepi. Through pumps to pulp: greening the paper industry's heat, 2023. [Online]. Available: https://ehpa.org/news-and-resources/publications/through-pumps-to-pulp-greening-the-paper-industrys-heat/. [Accessed 08 10 2025].
[3] Mujumdar A. S. *Handbook of industrial drying*. 3rd ed. Buca Raton: CRC Press, 2006.
[4] Li J, Liang Q.-C, Bennamoun L. Superheated steam drying: Design aspects, energetic performances, and mathematical modeling. *Renewable and Sustainable Energy Reviews* 2016; **60**, p. 1562-1583.
[5] Kiiskinen H, Edelmann K. Superheated Steam Drying of Paper Web. *Developments in Chemical Engineering and Mineral Processing* 2002; **10**: 3-4, p. 349-365.
[6] Dassault System. Dymola, 2025. [Online]. Available: https://www.3ds.com/de/products/catia/dymola. [Accessed 28 10 2025].
[7] TIL Energy. TIL Suite, 2025. [Online]. Available: https://tlk-energy.de/software/til-suite. [Accessed 28 10 2025].
[8] Godin H, Radgen P. Model-based framework for the evaluation of energy-efficiency measures in multi-cylinder paper drying. *Drying Technology* 2022; **40**:13, p. 2723–40.
[9] VDI-Gesellschaft Verfahrenstechnik und Chemieingenieurwesen. *VDI-Wärmeatlas*. Berlin: Springer Vieweg, 2013.
[10] Sun W, Braatz R D. ALVEN: Algebraic learning via elastic net for static and dynamic nonlinear model identification. *Computers & Chemical Engineering* 2020, **143**.
[11] Baehr H, Stephan K. *Wärme- und Stoffübertragung*, 2nd ed. Berlin: Springer, 1996.
[12] Shah M. A general correlation for Heat Transfer during film condensation inside pipe. *Int. J. Heat Mass Transfer* 1979; **22**, p. 547-556.
[13] Steimle S. *Refrigeration Technology Handbook (in German: Handbuch der Kältetechnik*, 2nd ed. Berlin: Springer, 1988.